Available online at www.sciencedirect.com
ScienceDirect
Ceramics International 35 (2009) 1661–1666
CERAMICS INTERNATIONAL
www.elsevier.com/locate/ceramint

Short communication

Preparation, structural and thermo-mechanical properties of lithium aluminum silicate glass–ceramics

A. Arvind [a], Rakesh Kumar [a], M.N. Deo [b], V.K. Shrikhande [a], G.P. Kothiyal [a,*]

[a] *Technical Physics & Prototype Engineering Division, Bhabha Atomic Research Centre, Mumbai 85, India*
[b] *High Pressure Physics Division, Bhabha Atomic Research Centre, Mumbai 85, India*

Received 8 May 2008; received in revised form 31 May 2008; accepted 17 July 2008
Available online 8 August 2008

Abstract

Lithium aluminum silicate glasses of composition (wt%) $12.6Li_2O$–$71.7SiO_2$–$5.1Al_2O_3$–$4.9K_2O$–$3.2B_2O_3$–$2.5P_2O_5$ were prepared by the melt quench technique. These glasses were converted to glass–ceramics based on DTA data. X-ray diffraction (XRD) and Fourier transform infra-red spectroscopy (FTIR) were used to discern the phases evolved in the glass–ceramics. Phase morphology was studied using scanning electron microscopy (SEM). Thermal expansion coefficient (TEC) and glass transition temperature (T_g) of all samples were measured using thermo-mechanical analyzer (TMA). It was found that 3 h dwell time at crystallization temperature yielded samples with good crystallinity with a TEC of $9.461 \times 10^{-6}\,^{\circ}C^{-1}$. Glass–ceramic-to-metal compressive seal with SS-304 was fabricated using LAS glass–ceramic. The presence of metal housing and compressive stresses at the glass–ceramic-to-metal interface reduced average grain size and changed the overall microstructure.

Keywords: B. Grain size; C. Hardness; C. Thermal expansion; D. Glass–ceramics

1. Introduction

Lithium aluminum silicate (LAS) glass–ceramics posses a range of useful properties such as high strength, good resistance to mechanical and thermal shocks and excellent chemical durability [1–3]. As a result LAS glass–ceramics see extensive application in heat exchangers, cookware, telescope mirror supports etc. [4,5]. The low alumina region of the LAS phase diagram yields lithium disilicate glass–ceramics [6]. These high strength, high thermal expansion coefficient (TEC) glass–ceramics are useful in hermetic sealing and enameling with high TEC metals. To precisely tune the TEC and other thermo-mechanical properties, heat-treatment schedule for crystallization must be carefully optimized. In this paper, we present some studies on the nature and morphology of crystalline phases formed in LAS glasses as a function of dwell time at crystallization temperature (T_d) using X-ray diffraction (XRD) and scanning electron microscopy (SEM). The effect of these phases on TEC (α), softening temperature and microhardness (μ-hardness) of the glass–ceramics is studied. As a technology demonstration, LAS glass–ceramic-to-metal (SS-304) compressive seal was fabricated. The glass–ceramic-to-metal interface was studied by using SEM and EDAX to understand the sealing mechanism and the effect of the metal housing on the morphology of the phases formed.

2. Experimental procedure

2.1. Preparation and characterization of glass–ceramics

LAS parent glasses of composition (wt%) $12.6Li_2O$–$71.7SiO_2$–$5.1Al_2O_3$–$4.9K_2O$–$3.2B_2O_3$–$2.5P_2O_5$ were prepared by the melt quench technique. Analytical grade precursors (Li_2CO_3, Al_2O_3, SiO_2, B_2O_3, $NH_4H_2PO_4$ and KNO_3) were mixed thoroughly and calcined in recrystallized alumina crucibles according to a schedule determined by the decomposition temperatures of the precursors. To ensure complete decomposition of nitrates and carbonates into oxides, the batch was weighed before and after calcination to ensure complete decomposition of the precursors. The calcined batch was melted under air ambient at 1500 °C in a Pt–Rh crucible in a raising lowering hearth electric furnace (Model OKAY R-70 M/s Bysakh and Co., Kolkata). After homogenization for 1 h, the melt was poured onto pre-heated graphite moulds and

* Corresponding author.
E-mail address: gpkoth@barc.gov.in (G.P. Kothiyal).

0272-8842/$34.00
doi:10.1016/j.ceramint.2008.07.019

Table 1
A summary of heat-treatment applied to various samples

Sample number	First crystallization temperature T_1 (°C)	Dwell time at T_1 (h)	Second crystallization temperature T_2 (°C)	Dwell time at T_2 (h)
LAS-A	600	2	800	2
LAS-B	600	2	800	3
LAS-C	600	2	800	4
LAS-D	600	2	800	5

annealed at 500 °C for a 3–4 h to relieve thermal stresses. The vitreous nature of the annealed glass was verified by powder XRD (Philips PW1710 X-Ray Diffractometer with collimated Cu Kα radiation).

DTA measurements on glass powders were performed on a Setaram 92-15 TG/DTA apparatus that was calibrated using the melting points of high purity indium and zinc. The non-isothermal experiments were performed by heating approximately 40 mg of the sample in Pt crucibles under protective ambient, using empty Pt crucible as reference. A heating rate of 10 K/min was employed in the range 25–1000 °C. Samples were crystallized according to DTA data. Samples were nucleated at 500 °C for 1 h and were then heated at 60 °C/h to 600 °C. After holding there for 2 h, samples were heated at 60 °C/h to 800 °C. Samples were held at that temperature for 2–5 h followed by furnace cooling to room temperature. The crystallization heat-treatments employed are given in Table 1. Powder XRD in the $20^\circ \leq 2\theta \leq 70^\circ$ range in steps of 0.5° was used to identify the crystalline phases formed. Phase identification was carried out using MATCH® software. Glass and glass–ceramic powders were mounted in KBr pellet for Fourier transform infra-red (FTIR) spectroscopy in the 40–1500 cm^{-1} range using a Bomem D8 Fourier transform spectrometer. To study phase morphology of unconstrained glass–ceramic samples, they were etched (10% HF for 10 s) and coated with gold. Secondary electron micrographs were taken on these samples using SEM (Vega MV2300T/40).

Glass as well as glass–ceramic samples were made flat by polishing and used for thermo-mechanical analysis (TMA) (Model 92-12 M/s Setaram, France). TMA was employed to measure the thermal expansion coefficient, glass transition temperature (T_g). The experiments were carried out in a precisely controlled furnace under flowing Ar ambient. Sample expansion was measured using a hemispherical silica probe with the sample under compressive load of 5 g.

Microhardness measurements were performed on mirror polished glass and glass–ceramic samples by a Vicker's microhardness tester (Model VMHT 30 M M/s Leica). In all cases, an indentation load of 100 g for 10 s was employed. Vicker's microhardness number (VHN) was calculated by measuring the diagonal length of the indentation made in the sample by a square base pyramidal indenter [7,8]. The VHNs reported are the averaged values for at least 10 indentations.

2.2. Seal fabrication and characterization

Compressive seal of LAS glass–ceramic with SS304 metal housing was prepared as per details discussed elsewhere [9]. The dwell time at crystallization temperature of 800 °C was maintained 3 h. The interface of the glass–ceramic-to-metal seal (constrained) has been studied by SEM as mentioned earlier.

3. Results

The LAS compositions studied yielded transparent bubble free glass. Powder XRD patterns of annealed LAS glasses showed the characteristic broad peaks of amorphous materials. Parent LAS glasses had a TEC of 10.5×10^{-6} °C^{-1} and T_g of

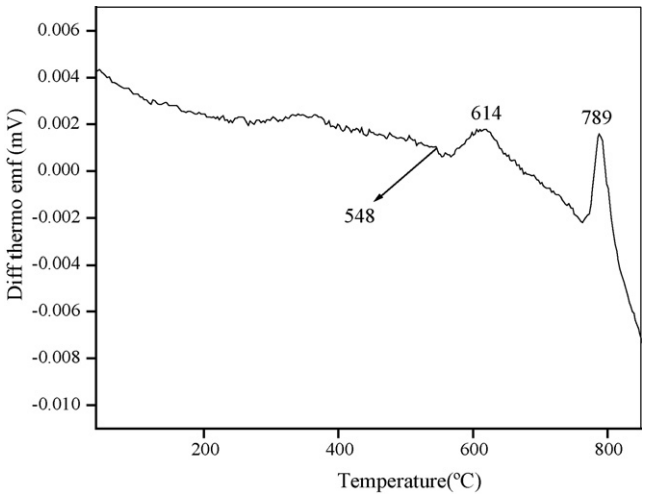

Fig. 1. DTA curve of LAS glass sample.

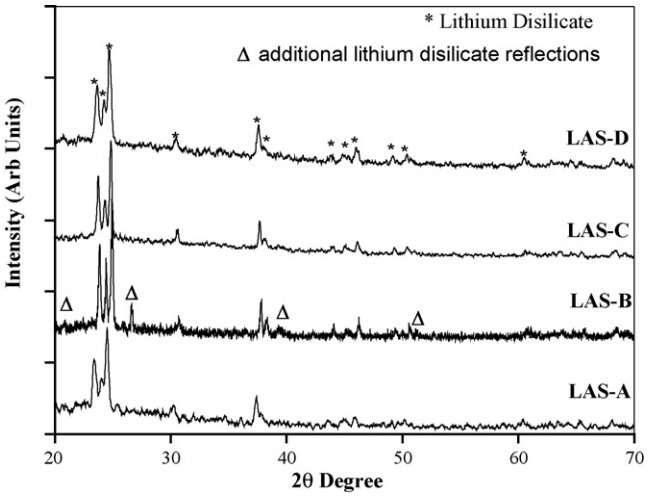

Fig. 2. XRD spectra of glass samples heat-treated at 800 °C for different dwell times. The extra peaks corresponding to lithium disilicate are indicated.

543 °. DTA curve of LAS glass is given in Fig. 1. It exhibits a glass transition endotherm at ∼550 °C and two well-defined exotherms at ∼600 and 800 °C. XRD spectra for samples heat-treated at 800 °C for various times are given in Fig. 2. Lithium disilicate was the major phase identified by XRD in all samples. Sample crystallinity seemed to increase with dwell time up to 3 h. This is borne out by the fact that the XRD spectrum of LAS-B glass–ceramic shows some additional peaks corresponding to lithium disilicate. The FTIR spectra for LAS parent glass and glass–ceramics are given in Fig. 3. Parent glasses show a strong peak characteristic of Si–O stretching modified by Al^{3+} as a cation coordinating the oxygen at 1000–1100 cm^{-1}. The peaks at 925 and 850 cm^{-1} can be attributed to the presence of non-bridging oxygen (NBO) atoms, while the absorbance at ∼730 cm^{-1} arises due to the Al–O covalent bond vibration caused by Al^{3+} substituting isomorphously for Si^{4+} [10,11]. The FTIR spectra for glass–ceramics heat-treated for 2 h (a), 3 h (b) and 5 h (c) show strong peaks at ∼550, 640, 755, 785 and 935 cm^{-1} corresponding to lithium disilicate. Additional peaks

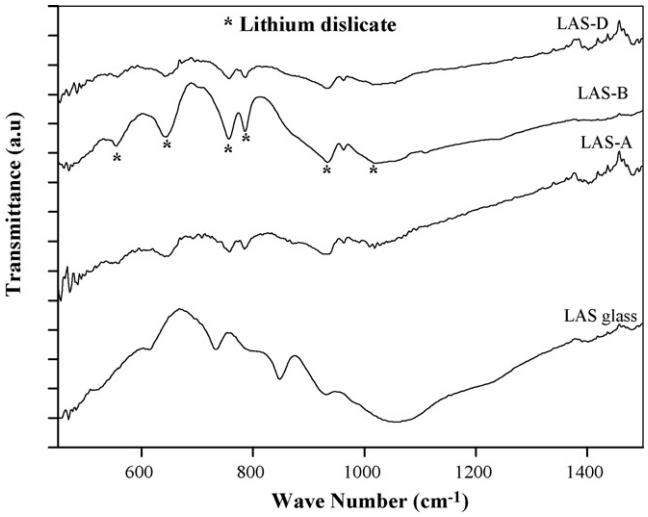

Fig. 3. FTIR spectra of LAS glass (bottom) and LAS glass–ceramics heat-treated at 800 °C for 2 h (LAS-A), 3 h (LAS-B) and 5 h (LAS-D).

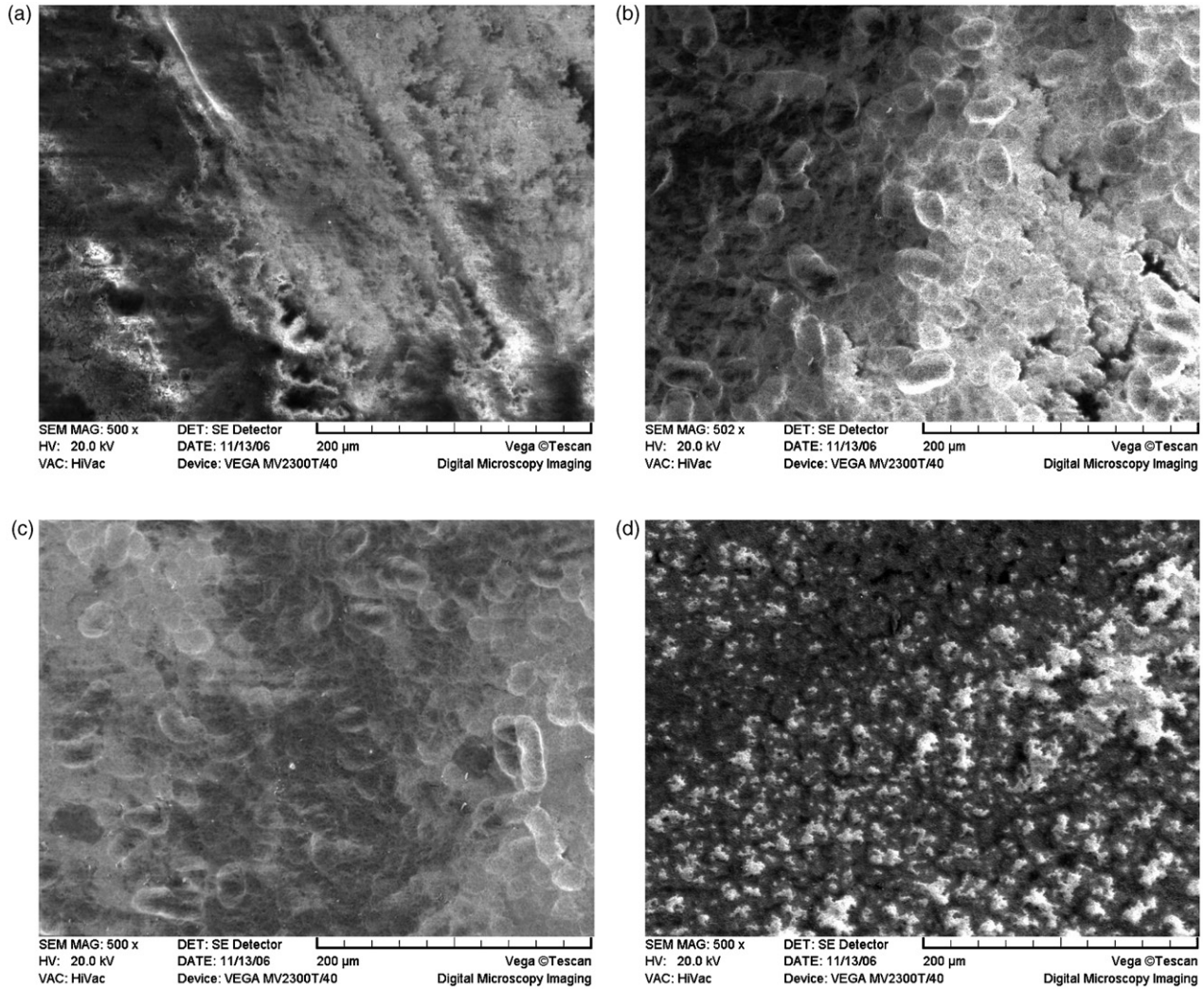

Fig. 4. SEM micrographs of unconstrained LAS samples heat-treated at 800 °C for (a) 2 h, (b) 3 h, (c) 4 h and (d) 5 h.

Table 2
Thermo-physical properties of LAS glass–ceramics heat-treated at 800°C for 2–5 h

Sample number	Dwell time at 800 °C (h)	TEC ($\times 10^{-6}$ °C^{-1})	T_g (°C)	μH (Gpa)
LAS-A	2	8.397	573	6.47 ± 0.05
LAS-B	3	9.461	584	6.62 ± 0.05
LAS-C	4	8.896	544	6.79 ± 0.05
LAS-D	5	8.962	582	6.84 ± 0.05

corresponding to the same phase were observed in LAS-B glass–ceramics at ∼470 and 1018 cm^{-1} [12]. In addition, the absorption peaks in LAS-B sample are more sharp and well-defined implying greater crystallinity in this glass–ceramic. SEM micrographs of LAS-A, -B, -C and -D glass–ceramics (unconstrained) are given in Fig. 4. At 3 h dwell time, as is evident from Fig. 4b, a highly crystalline sample is obtained with an ovoidal microstructure of lithium disilicate with an average grain size of 20–30 μm. The microstructure of samples heat-treated beyond 3 h shows signs of phase melting. The associated

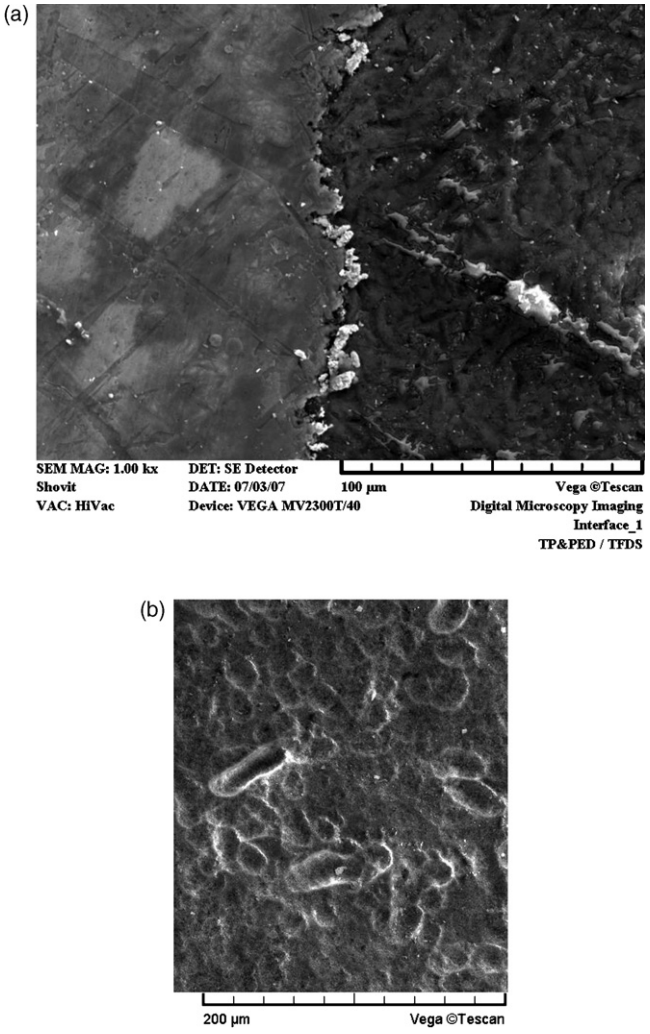

Fig. 5. SEM micrograph of (a) the glass–ceramic-to-metal interface showing the effect of the compressive stress on microstructure of the LAS glass–ceramic and (b) the centre of the seal.

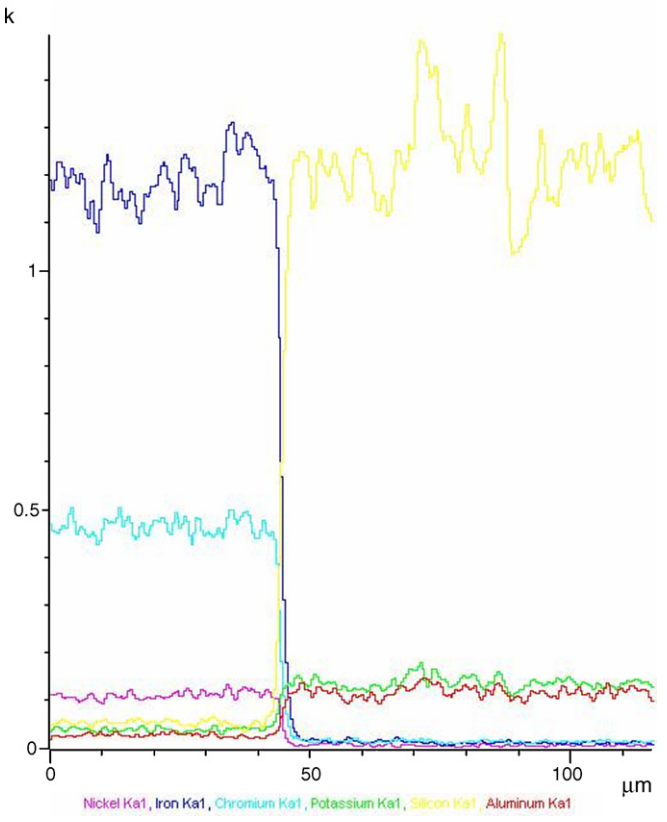

Fig. 6. EDAX line scan across the glass–ceramic-to-metal interface showing no interdiffusion of species.

changes in thermo-physical properties are given in Table 2. Glass–ceramics heat-treated at 800 °C for 3 h have the highest TEC and T_g of all glass–ceramics prepared. Microhardness of all glass–ceramics were higher than parent glass and increased slowly with dwell time. SEM micrograph of the glass–ceramic-to-metal seal interface is shown in Fig. 5a. The microstructure at the interface is strongly influenced by the presence of the metal housing. The average grain size in the presence of the metal is smaller (10–15 μm) than LAS-B glass–ceramics (unconstrained) (20–30 μm). In addition to the reduction in grain size, phase morphology changes at the glass–ceramic-to-metal interface. The microstructure at the interface is made up of fine, rounded grains and a few whisker like grains extending towards the glass–ceramic region. At the centre of the seal, microstructure (Fig. 5b) was quite similar to that of the unconstrained glass–ceramic (Fig. 4b). EDAX line scans (Fig. 6) run across the glass–ceramic-to-metal interface show no inter-diffusion of species. Leak tests performed on the seal showed it to be capable of withstanding a vacuum of 1.33×10^{-4} Pa at a helium leak rate of less than 1.33×10^{-10} Pa m^3/s. The seal also withstood a pressure of 82.73 MPa.

4. Discussion

The LAS glass composition chosen for this study lies in the low alumina, lithium disilicate yielding region of the LAS phase diagram [6]. The P_2O_5 added to the composition causes

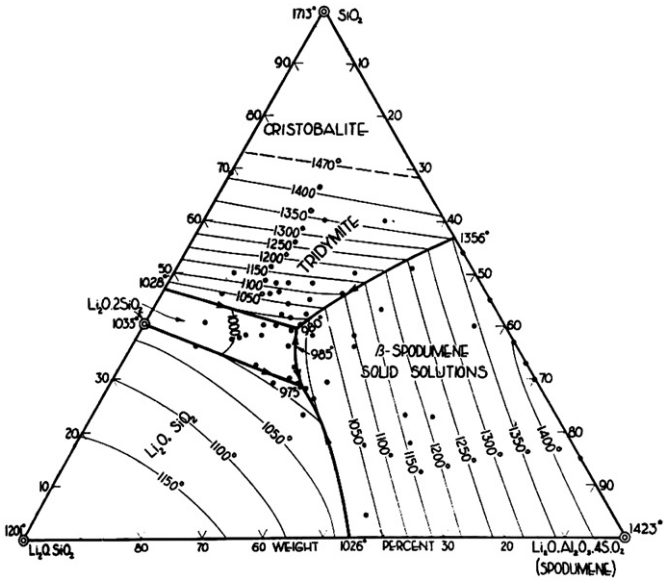

Fig. 7. Li_2O–Al_2O_3–SiO_2 phase diagram showing the low eutectic temperature in the lithium disilicate forming region (reproduced from Ref. [6]).

the crystallization of Li_3PO_4 crystallites. These then act as sites for heterogeneous crystallization of cristobalite and lithium metasilicate as has been earlier observed by Headley and Loehman [13] and Arvind et al. [14]. This gives rise to the DTA exotherm observed around 600 °C. Lithium metasilicate then reacts with cristobalite to yield lithium disilicate [15,16] leading to the DTA exotherm at around 800 °C. Therefore, heat-treatment at 600 °C followed 800 °C results in lithium disilicate as the major crystalline phase in all glass–ceramics prepared. The lithium metasilicate phase is thermodynamically unstable but kinetically favourable and this phase appears first. On heat-treatment at higher temperature, this phase is replaced by the slower growing, but thermodynamically favoured lithium disilicate phase [17]. From the LAS phase diagram (Fig. 7), it is evident that the lowest eutectic of low alumina LAS compositions is around 1000 °C [6,18]. The addition of fluxes such as B_2O_3 and K_2O to aid melting will reduce this even further. The lowered eutectic would reduce the activation energy for diffusion and allow faster growth of lithium disilicate phase. At the same time, prolonged heat-treatment at 800 °C could lead to phase melting. Therefore, on heat-treatment up to 3 h, sample crystallinity increases. Beyond this, phase melting commences as evident in XRD and FTIR spectra and confirmed by SEM micrographs. Up to 3 h dwell time, TEC of the samples increases progressively due to the crystallization of high TEC lithium disilicate phase. Beyond this dwell time, lithium disilicate phase melts and causes TEC to reduce. In view of this, a dwell time of 3 h at 800 °C is optimum for achieving comparatively higher sample crystallinity.

As mentioned earlier, the precipitated Li_3PO_4 aggregates in the melt during seal formation act as nucleation sites. In addition, the presence of metal near glass (glass–ceramic)-to-metal interface also contributes to nucleation sites. This leads to an enhancement in nucleation rate leading to greater number of nuclei close to the interface. These nuclei grow to form smaller crystallites during glass–ceramic transformation as has been observed in case of lithium zinc silicate glass–ceramic-to-metal seal [8]. In this case we have an additional factor of radial compressive stress at the interface due to the mismatch in TEC between metal and glass–ceramic (compressive seal). This also checks the growth of crystallites resulting in further decrease in grain size. This is in agreement with reports of reduction in crystallite size under pressure by Fuss et al. [19]. Further due to the combined effect of presence of metal and compressive stress, some whisker like growths near the interface also takes place with an overall modification of microstructure. As we move towards the centre of the seal, the effects of metal and compressive stress diminish and growth of crystallites of nearly same size and morphology as in case of unconstrained situation (Fig. 4b) are observed. Since the seal formed was of the compressive (unmatched) type leak tightness between metal and glass–ceramic was established as a result of high compressive stress and hence, there was no interdiffusion of species between glass–ceramic and metal as is normally observed in a matched type seal.

5. Conclusions

We observe that dwell time at crystallization temperature has a profound effect on the evolution of microstructure. A dwell time of 3 h at crystallization temperature results in a high TEC glass–ceramic with a comparatively high T_g. The glass–ceramic-to-metal seal was of the compressive type and could withstand a vacuum of 1.33×10^{-4} Pa at a helium leak rate of less than 1.33×10^{-10} Pa m^3/s. The seal was found capable of withstanding a high pressure of 82.73 MPa. The presence of the metal housing and compressive stresses at the glass–ceramic-to-metal interface greatly affect the morphology of phases formed.

Acknowledgements

The authors wish to thank Drs V.C. Sahni and J.V. Yakhmi for their support and encouragement. Thanks are also due to Dr. Shovit Bhattacharya and Mr. Thinaharan for SEM measurements. The technical support of M/s. H.Y. Bodari, P.A. Wagh and Y.B. Shirkar is gratefully acknowledged. One of the authors (AA) would like to thank the DAE for awarding him a fellowship.

References

[1] H. Zhaoxia, S. Chunhui, Z. Yongming, Z. Huashan, Z. Hongbo, S. Jing, M. Qingxin, Effect of crystallization of Li_2O–Al_2O_3–SiO_2 glasses on luminescence property of Nd^{3+} ions, J. Rare Earths 24 (2006) 418–422.
[2] P. Riello, P. Canton, N. Comelato, S. Polizi, M. Verità, G. Fagherazzi, H. Hofmeister, S. Hopfe, Nucleation and crystallization behaviour of glass–ceramic material in the Li_2O–Al_2O_3–SiO_2 system of interest for their transparency properties, J. Non-Cryst. Solids 288 (2001) 127–139.
[3] M. Chatterjee, M.K. Naskar, Sol–gel synthesis of lithium aluminum silicate powders: the effect of silica source, Ceram. Int. 32 (2006) 623–632.

[4] B. Karmakar, P. Kundu, S. Jana, R.N. Dwivedi, Crystallization kinetics and mechanisms of low-expansion lithium-alumino silicate glass–ceramics by dilatometry, J. Am. Ceram. Soc. 85 (10) (2002) 2572–2574.
[5] K. Cheng, Carbon effects on the crystallization of Li_2O–Al_2O_3–SiO_2 glasses, J. Non-Cryst. Solids 238 (1–2) (1998) 152–157.
[6] M.K. Reeser (Ed.), Phase diagrams for ceramists Am. Ceram. Soc. (Columbus, OH) (1969) 166–168, Figs. 445–449.
[7] M. Yamane, J.D. Mackenzie, Vicker's hardness of glass, J. Non-Cryst. Solids 15 (2) (1974) 153–164.
[8] B.I. Sharma, M. Goswami, P. Sengupta, V.K. Shrikhande, G.B. Kale, G.P. Kothiyal, Study on some thermo-physical properties in Li_2O–ZnO–SiO_2 glass–ceramics, Mater. Lett. 58 (19) (2004) 2423–2428.
[9] A. Arvind, R. Kumar, S. Bhattacharya, V.K. Shrikhande, G.P. Kothiyal, Some properties of lithium aluminium silicate (LAS) glass–ceramics used in glass–ceramic to metal compressive seal for vacuum applications, J. Phys. Conf. Ser. 114 (2008) 012042.
[10] B.N. Roy, Spectroscopic analysis of the structure of silicate glasses along the joint $x\mathrm{MAlO_2}$–$(1-x)\mathrm{SiO_2}$ (M = Li, Na, K, Rb, Cs), J. Am. Ceram. Soc. 70 (3) (1987) 183–192.
[11] M.K. Naskar, M. Chatterjee, A novel process for the synthesis of lithium aluminum silicate powders from rice husk ash and other water based precursor materials, Mater. Lett. 59 (2005) 998–1003.
[12] T. Fuss, A. Moguš-Milanković, C.S. Ray, C.E. Lesher, R. Youngman, D.E. Day, Ex situ XRD, TEM, IR, Raman and NMR spectroscopy of crystallization of lithium disilicate glass at high pressure, J. Non-Cryst. Solids 352 (2006) 4101–4111.
[13] T.J. Headley, R.J. Loehman, Crystallization of a glass–ceramics by epitaxial growth, J. Am. Ceram. Soc. 67 (9) (1984) 354–361.
[14] A. Arvind, A.K. Tyagi, R. Mishra, V.K. Shrikhande G.P. Kothiyal, Evolution of crystalline phases as a function of composition and dwell time in lithium aluminum silicate glass–ceramics, Phys. Chem. Glasses, in press.
[15] W. Höland, E. Apel, Ch. Van't Hoen, V. Rheinberger, Studies of crystal phase formation in high strength lithium disilicate glass–ceramics, J. Non-Cryst. 352 (38–39) (2006) 4041–4050.
[16] M. Goswami, P. Sengupta, K. Sharma, R. Kumar, V.K. Shrikhande, J.M.F. Ferreira, G.P. Kothiyal, Crystallization behaviour of Li_2O–ZnO–SiO_2 glass–ceramic system, Ceram. Int. 33 (5) (2007) 863–867.
[17] L.L. Burgner, P. Lucas, M.C. Weinberg, P.C. Soares Jr., E.D. Zanotto, On the persistence of metastable phases in lithium disilicate glass, J. Non-Cryst. Solids 274 (2000) 188–194.
[18] M.P. Borom, A.M. Turkalo, R.H. Doremus, Strength and microstructure in lithium disilicate glass–ceramics, J. Am. Ceram. Soc. 58 (9–10) (1975) 385–391.
[19] T. Fuss, C.S. Ray, C.E. Lesher, D.E. Day, In situ crystallization of lithium disilicate glass: effect of pressure on crystal growth rate, J. Non-Cryst. Solids 352 (2006) 2073–2081.